ISSN 2070-2051, Protection of Metals and Physical Chemistry of Surfaces, 2017, Vol. 53, No. 3, pp. 534–547. © Pleiades Publishing, Ltd., 2017.

NEW SUBSTANCES, MATERIALS AND COATINGS

Kinetics of Boron Diffusion and Characterization of Fe_2B Layers on AISI 9840 Steel[1]

M. Ortiz-Domínguez[a], O. A. Gómez-Vargas[b], M. Keddam[c, *], A. Arenas-Flores[d], and J. García-Serrano[d]

[a] *Universidad Autónoma del Estado de Hidalgo, Escuela Superior de Ciudad Sahagún-Ingeniería Mecánica, Carretera Cd. Sahagún-Otumba s/n, Zona Industrial CP. 43990, Hidalgo, México*

[b] *Instituto Tecnológico de Tlalnepantla-ITTLA. Av., Instituto Tecnológico, S/N. Col. La Comunidad, Tlalnepantla de Baz. CP. 54070. Estado de México, México*

[c] *Laboratoire de Technologie des Matériaux, Faculté de GénieMécanique et Génie des Procédés, USTHB, B.P. No. 32, 16111 El-Alia, Bab-Ezzouar, Algiers, Algeria*

[d] *Universidad Autónoma del Estado de Hidalgo-AACTyM, Carretera Pachuca Tulancingo Km. 4.5, Mineral de la Reforma. CP. 42184. Hidalgo, México*

**e-mail: keddam@yahoo.fr, mkeddam@usthb.dz*

Received January 22, 2016

Abstract— In this work, the AISI 9840 steel was subjected to the powder-pack boriding in the temperature range of 1123–1273 K for various times ranging from 2 to 8 h. A kinetic model based on the principle of mass conservation at the growing interface was used to estimate the boron diffusion coefficients through the Fe_2B layers. The pack-borided samples were experimentally characterized by different techniques such as: Scaning electron microscopy, XRD analysis, Microhardness Vickers testing. The Daimler-Benz Rockwell-C indentation technique was used to assess the adhesion quality of boride coatings on AISI 9840 steel. Finally, the scratch and pin-on-disc tests for wear resistance were respectively performed using an LG Motion Ltd and a CSM tribometer under dry sliding conditions. The boron activation energy for the AISI 9840 steel was estimated as 193.08 kJ /mol by applying the present model. To confirm and extend the validity of the diffusion model, the experimental values of Fe_2B layers thicknesses obtained for other boriding conditions were compared with the predicted values.

DOI: 10.1134/S2070205117030169

NOMENCLATURE

v is the boride layer thickness, m.

k_{Fe_2B} is the rate constant in the Fe_2B phase, m/s $^{1/2}$.

t_v is the effective growth time of the Fe_2B layer, s.

t is the treatment time, s.

$t_0^{Fe_2B}$ is the boride incubation time, s.

$C_{up}^{Fe_2B}$ represents the upper limit of boron content in Fe_2B ($= 60\times10^3$ mol/m^3).

$C_{low}^{Fe_2B}$ is the lower limit of boron content in Fe_2B ($= 59.8\times10^3$ mol/m^3).

C_{ads}^{B} is the adsorbed boron concentration in the boride layer, mol/m^3.

$a_1 = C_{up}^{Fe_2B} - C_{low}^{Fe_2B}$ defines the homogeneity range of the Fe_2B layer (mol/m^3).

$a_2 = C_{low}^{Fe_2B} - C_0$ is the miscibility gap, mol/m^3.

C_0 is the terminal solubility of the interstitial solute ($\approx$0 mol/m^3).

$C_{Fe_2B}[x(t)]$ is the boron concentration profile in the Fe_2B layer, mol/m^3.

ε is the normalized growth parameter for the (Fe_2B/substrate) interface (it has no physical dimension).

D_{Fe_2B} represents the diffusion coefficient of boron in the Fe_2B phase, m^2/s.

$J_i[x(t)]$, (with i = Fe_2B and Fe) are the fluxes of boron atoms in the (Fe_2B /substrate) interface boundary (mol/m^2 s).

1. INTRODUCTION

The boriding treatment is a thermochemical process in which boron atoms are diffused into the material substrate to get a hard boride layer composed of borides.

[1] The article is published in the original.

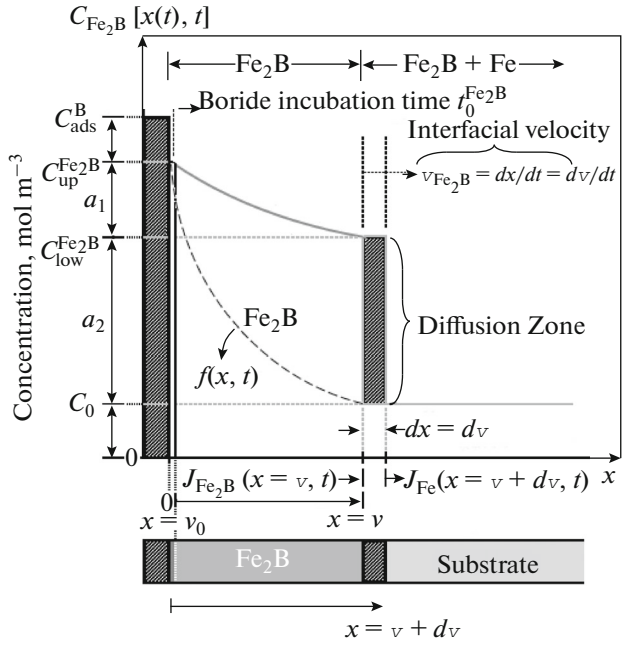

Fig. 1. A schematic boron-concentration profile through the Fe_2B layer.

The boriding treatment requires a high temperature ranging from 800 to 1000°C and process time between 0.5 and 8 h [1]. This thermochemical process can be applied to ferrous alloys [2–7] and non-ferrous alloys [8–13]. In case of steels and Armco iron, the boride layer formed on steel may consist of either a single-phase (Fe_2B) or ($FeB + Fe_2B$). These iron borides are characterized by many advantageous properties such as: a high surface hardness, a high abrasive wear resistance, corrosion resistance and oxidation resistance at temperatures of up to 850°C. The main disadvantage of boriding is the brittleness of the boride layer, especially the FeB phase.

The formation of a single phase Fe_2B is more desirable than a double-phase layer ($FeB + Fe_2B$).

The boron-rich FeB phase is considered not suitable since the FeB phase is more brittle than Fe_2B. Its brittleness leads to flaking and spalling when subjected to thermal and/or mechanical shock. The boride layer thickness formed on the steel surface, depends on various factors such as: the boriding method, the boriding parameters and the quantity of active boron available in the boriding medium.

From a kinetic point of view, some recent diffusion models, regarding the growth of Fe_2B layers on different substrates, were reported in the literature [14–27]. These approaches considered the effect of boride incubation times and can be used to select the optimum boride layers thicknesses according to the industrial applications of the borided materials. The pack boriding treatment was employed to improve the tribological properties and extend the lifetime of the workpieces made of AISI 9840 steel.

The objective of this work was to investigate the boriding kinetics of AISI 9840 steel and its tribological behaviour.

No study has been reported till now in the literature about the growth of boride layers and the modeling of boriding kinetics of AISI 9840 steel. For this purpose, an original diffusion model taken from the reference work [21] was then adopted for investigating the boriding kinetics of AISI 9840 steel. The present model assumes a non linear boron concentration profile through the Fe_2B layer with a value of the lower limit of boron content in Fe_2B depending on the process temperature. In addition, the present model includes the effect of boride incubation time, which is independent on the boriding temperature, during the formation of Fe_2B layer on AISI 9840 steel. A diffusion model was then applied to estimate the boron activation energy for the AISI 9840 steel basing on our experimental data. The Fe_2B layers formed on the AISI 9840 steel were characterized by different experimental techniques such as: Scanning electron microscopy (SEM), XRD analysis, and microhardness Vickers testing.

The Daimler-Benz Rockwell-C indentation technique was used to asses the cohesion of boride coating formed on the AISI 9840 steel.

In addition, the scratch and pin- on-disc tests for wear resistance were respectively performed using an LG Motion Ltd and a CSM tribometer under dry sliding conditions (in ambient air at room temperature). Finally, a comparison was made between the borided and unborided samples regarding the wear behaviour and evolution of friction coefficient.

2. THE DIFFUSION MODEL

2.1. The Mass Balance Equation

The model considers the formation of Fe_2B layer on a saturated substrate with boron atoms as depicted in Fig. 1.

The $f(x,t)$ function gives the distribution of boron concentration in the substrate before the nucleation of Fe_2B phase. $t_0^{Fe_2B}$ represents the incubation time of Fe_2B phase when a saturation state is attained within the matrix. $C_{up}^{Fe_2B}$ defines the upper limit of boron content in Fe_2B ($= 60\times10^3$ mol m^{-3}), while $C_{low}^{Fe_2B}(T)$ represents the lower limit of boron content in $Fe_2B = (-0.0004T + 60.373)\times10^3$ mol/m^3. The point $x(t = t) = v$ is the thickness of Fe_2B layer [28]. The term C_{ads}^{B} is the effective adsorbed boron concentration or the effective boron concentration during the boriding process [29]. The activation energy associ-

ated with the adsorption phenomenon depends on the surface coverage of adsorbed species. When the adsorbed boron concentration is sufficient on the sample surface, the Fe_2B layer is formed and proceeds to grow. The parameter $a_1 = C_{up}^{Fe_2B} - C_{low}^{Fe_2B}(T)$ defines the homogeneity range of Fe_2B layer, while $a_2 = C_{low}^{Fe_2B}(T) - C_0$ is the miscibility gap. The term C_0 represents the boron solubility in the matrix which is very low and can be neglected [30, 31].

The assumptions taken during the formulation of diffusion model are the following:

– The growth kinetics is controlled by the boron diffusion in the Fe_2B layer.

– The Fe_2B phase nucleates after a specific incubation time.

– The Fe_2B layer grows because of the boron diffusion perpendicular to the specimen surface.

– Boron concentrations remain constant in the boride layer during the treatment.

– The influence of the alloying elements on the growth kinetics of the layer is not taken into account.

– The boride layer is thin compared to the sample thickness.

– A uniform temperature is assumed throughout the sample.

– Planar morphology is assumed for the phase interface.

The initial and boundary conditions for the diffusion problem are represented as:

$$t = 0, x > 0, \text{ with: } C_{Fe_2B}[x(t), t = 0] = C_0 \approx 0. \quad (1)$$

Boundary conditions:

$$\left.\begin{aligned} &C_{Fe_2B}\left[x\left(t = t_0^{Fe_2B}\right) = v_0, t = t_0^{Fe_2B}\right] = C_{up}^{Fe_2B} \text{ (the upper boron concentration is kept constant)},\\ &\text{for } C_{ads}^{B} > 60\times10^{3} \text{ mol m}^{-3}, \end{aligned}\right\} \quad (2)$$

$$\left.\begin{aligned} &C_{Fe_2B}[x(t = t) = v,\ t = t] = C_{low}^{Fe_2B}(T) \text{ (the boron concentration at the interface is kept constant)},\\ &C_{ads}^{B} < 59.8\times10^{3} \text{ mol m}^{-3}, \end{aligned}\right\} \quad (3)$$

v_0 is a thin layer with a thickness of ≈5 nm that formed during the nucleation stage [32]. Thus $v_0(\approx 0)$ when compared to the Fe_2B layer thickness (v). The mass balance equation at the (Fe_2B/substrate) interface can be formulated by Eq. (4) as follows:

$$\left(\frac{C_{up}^{Fe_2B} + C_{low}^{Fe_2B}(T) - 2C_0}{2}\right)(Adv) = J_{Fe_2B}(x = v,\ t = t)(Adt) - J_{Fe}(x = v + dv,\ t = t)(Adt), \quad (4)$$

where $A(= 1\times1)$ is defined as the unit area. The flux J_{Fe_2B} and J_{Fe} are obtained from the Fick's First law as:

$$J_{Fe_2B}[x(t = t) = v,\ t = t] = -\left\{D_{Fe_2B}\partial C_{Fe_2B}[x(t = t) = v,\ t = t]/\partial x\right\}_{x=v}, \quad (5)$$

and

$$J_{Fe}[x(t = t) = v + dv,\ t = t] = -\left\{D_{Fe}\partial C_{Fe}[x(t = t) = v + dv,\ t = t]/\partial x\right\}_{x=v+dv} \quad (6)$$

The term J_{Fe} is null since the boron solubility in the matrix is very low (≈0 mol /m^3) [30, 31].

Thus, Eq. (4) can be written as:

$$\left(\frac{C_{up}^{Fe_2B} + C_{low}^{Fe_2B}(T) - 2C_0}{2}\right)\left.\frac{dx(t)}{dt}\right|_{x(t)=v} = -D_{Fe_2B}\left.\frac{\partial C_{Fe_2B}[x(t = t), t = t]}{\partial x}\right|_{x(t)=v}. \quad (7)$$

If the boron concentration profile in Fe_2B is constant for the treatment time, Fick's Second law is reduced to an ordinary second-order differential equation as follows:

$$\frac{\partial C_{Fe_2B}[x(t), t]}{\partial t} = D_{Fe_2B}\frac{\partial^2 C_{Fe_2B}[x(t), t]}{\partial x^2}. \quad (8)$$

By solving Eq. (8), and applying the boundary conditions proposed in Eqs. (2) and (3), the boron concentration profile in Fe_2B is expressed by Eq. (9) if the boron diffusion coefficient in Fe_2B is constant for a particular temperature:

$$C_{Fe_2B}[x(t), t] = C_{up}^{Fe_2B} + \frac{C_{low}^{Fe_2B}(T) - C_{up}^{Fe_2B}}{\operatorname{erf}\left(\frac{v}{2\sqrt{D_{Fe_2B}t}}\right)}\operatorname{erf}\left(\frac{x}{2\sqrt{D_{Fe_2B}t}}\right). \quad (9)$$

By substituting Eq. (9) into Eq. (7), Eq. (10) is obtained:

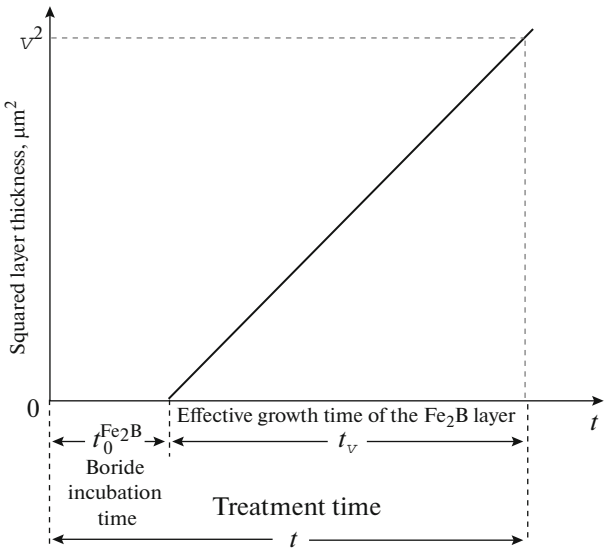

Fig. 2. A schematic representation of the square of the layer thickness as a function of the treatment time.

$$\left(\frac{C_{up}^{Fe_2B}+C_{low}^{Fe_2B}(T)-2C_0}{2}\right)\frac{dv}{dt} = \sqrt{\frac{D_{Fe_2B}}{\pi t}}\frac{C_{up}^{Fe_2B}-C_{low}^{Fe_2B}(T)}{\operatorname{erf}\left(\frac{v}{2\sqrt{D_{Fe_2B}t}}\right)}\exp\left(-\frac{v^2}{4D_{Fe_2B}t}\right), \quad (10)$$

for $0 \le x \le v$.

Substituting the expression of the parabolic growth law: ($v = 2\varepsilon D_{Fe_2B}^{1/2} t^{1/2}$) into Eq. (10), Eq. (11) is deduced:

$$\left(\frac{C_{up}^{Fe_2B}+C_{low}^{Fe_2B}(T)-2C_0}{2}\right)\varepsilon = \sqrt{\frac{1}{\pi}}\frac{C_{up}^{Fe_2B}-C_{low}^{Fe_2B}(T)}{\operatorname{erf}(\varepsilon)}\exp(-\varepsilon^2). \quad (11)$$

The normalized growth parameter (ε) for the (Fe_2B/substrate) interface can be estimated numerically by the Newton-Raphson method. It is assumed that expressions $C_{up}^{Fe_2B}$, $C_{low}^{Fe_2B}(T)$, and C_0, do not depend significantly on temperature (in the considered temperature range) [28].

A schematic representation of the square of the layer thickness against linear time $\left(v^2 = 4\varepsilon^2 D_{Fe_2B} t = 4\varepsilon^2 D_{Fe_2B}\left(t_v + t_0^{Fe_2B}\right)\right)$ is depicted in Fig. 2. $t_v\left(= t - t_0^{Fe_2B}\right)$ is the effective growth time of the Fe_2B layer and t is the treatment time.

3. EXPERIMENTAL PROCEDURE

3.1. The Boriding Process

The material that was borided was AISI 9840 steel. It had a nominal chemical composition of 0.38–0.43% C, 0.15–0.35% Si, 0.70–0.90% Mn, 0.70–0.90% Cr, 0.85–1.15% Ni, 0.10–0.30% V, 0.20–0.30% Mo, 0.040% P and 0.040% S. The samples were sectioned into cubes with dimensions of $10\times10\times10$ mm^3. Prior to the boriding process, the samples were polished, ultrasonically cleaned in an alcohol solution and deionized water for 15 min at room temperature, and dried and stored under clean-room conditions. The mean hardness of the substrate was 389 HV. The samples were embedded in a closed cylindrical case (AISI 304L), containing a fresh Durborid powder mixture. The powder mixture is composed of an active source of boron (33.5 wt % of B_4C), an inert filler (61.1 wt % SiC), and an activator (5.4 wt % of KBF_4). The active boron is then supplied by the powder quantity placed over and around the material surface. The boriding process was performed in a conventional furnace under a pure argon atmosphere. It was carried out in the temperature range of 1123–1273 K for a variable time (2, 4, 6 and 8 h). Once the treatment was complete, the container was removed from the furnace and slowly cooled to room temperature.

3.2. Experimental Techniques

The borided and etched samples were cross-sectioned, for microstructural observations under a scanning electron microscope (JEOL JSM 6300). For a kinetic study, the boride layer thickness was automatically measured with the aid of MSQ PLUS *software*. To ensure the reproducibility of the measured layers thicknesses, fifty measurements were collected in different sections of the borided AISI 9840 steel samples to estimate the Fe_2B layer thickness; defined as an average value of the long boride teeth [20, 21, 33]. All thickness measurements were taken from a fixed reference on the surface of the borided AISI 9840 steel. The phases of the boride layers were investigated by an X-Ray Diffraction (XRD) equipment (Equinox 2000) using CoK_α radiation of 0.179 nm wavelength. The Daimler-Benz Rocwell-C was performed to get a qualitative information on the adhesive strength of the boride layers to the substrate. The well-known Rockwell-C indentation test is prescribed by the VDI 3198 norm, as a destructive quality test of coated compounds [34–36]. The principle of this method was presented in Fig. 3 and reported in the reference work [36].

In this method, a conical diamond indenter penetrated into the surface of an investigated layer, thus inducing massive plastic deformation to the substrate and fracture of the boride layer. A load of 1471 N was applied to cause coating damage adjacent to the

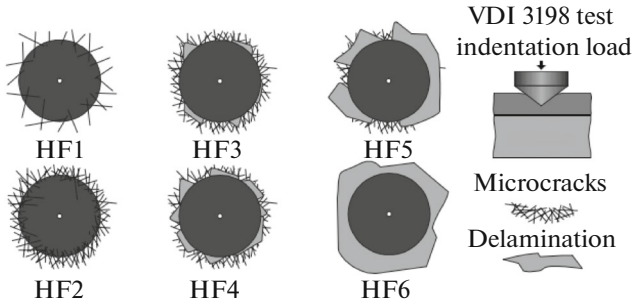

Fig. 3. Principle of the VDI 3198 indentation test [34].

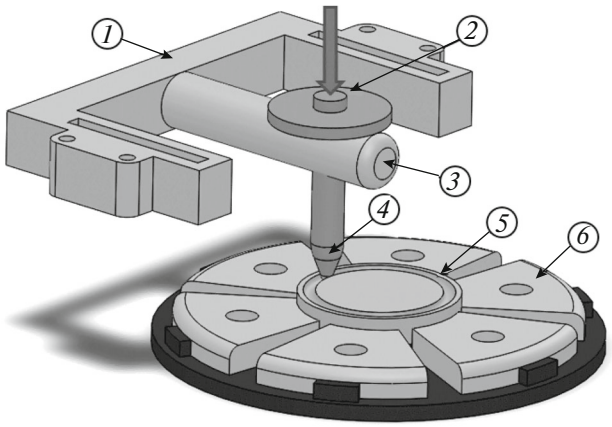

Fig. 4. Schematic diagram of typical pin-on-disc test device ((*1*) Elastic arm; (*2*) weight (1 N, 2 N, 5 N and 10 N); (*3*) friction force sensor; (*4*) pin, ball holders; (*5*) wear track; (*6*) rotating disc or cap for liquid testing).

boundary of the indentation. Three indentations were conducted for each borided sample and scanning electron microscopy (SEM) was used to assess the adhesion test. The damage to the boride layer was compared with the adhesion strength quality maps HF1-HF6 (see Fig. 3). In general, the adhesion strength HF1 to HF4 are defined as sufficient adhesion, whereas HF5 and HF6 represent insufficient adhesion [34]. The hardness of the boride layers was measured by means of a Vickers indenter with a load of 0.5 N, and the average value was taken as representative of the hardness. To evaluate the tribological properties of unborided and borided surface, samples with a diameter of 25.4 mm and a thickness of 10 mm were used and cleaned with acetone to remove contaminants from the surface. For tribological characterizations, two different techniques (pin-on-disc and scratch tests) were employed to characterize the wear resistance of boride layers on AISI 9840 steel. The pin-on-disc tests were carried out in dry sliding conditions using a CSM tribometer (see Fig. 4).

This machine is used to determine the magnitude of friction coefficient and wear as two surfaces rub together. In one measurement method a pin or a sphere is loaded onto the test sample with a precisely known force. The pin is mounted on a stiff lever, designed as a frictionless force transducer. The friction coefficient is determined during the test by measuring the deflection of the elastic arm. This simple method facilitates the study of friction and wear behavior of almost every solid state material combination with or without lubricant. Furthermore, the control of the test parameters such as speed, frequency, contact pressure, time and the environmental parameters (temperature, humidity and lubricant) allows simulation of the real life conditions of a practical wear situation. Tribological tests were performed using a diamond-made indenter with a 10 mm-diameter hemispheric. Wear test machine (CSM tribometer (pin-on-disc)) was used at room temperature with a relative humidity of 40%. All tests were conducted for a total sliding distance of 500 m with a sliding speed of 0.08 m/s and the covered radial distance was of 14 mm under a normal load 5 N. The scratch wear tests were achieved at ambient conditions without lubrication. To evaluate the tribological properties of unborided and borided surface of samples by the scratch test, the plates were cut into the dimension of $12 \times 12 \times 7$ mm^3 and were cleaned with acetone to remove contaminants from the surface. The test consists in scratching the sample surface by using a LG Motion Ltd (scratch) with a single-pass under increasing normal load at a rate of 10 N/mm of covered distance. Applied loads were between 0 and 90 N. This allows the determination of the critical load (L_c) corresponding to the apparition of the layer damage. The scratch tests were carried out in dry sliding conditions using a LG Motion Ltd (see Fig. 5).

The technique involves generating a controlled scratch with a sharp tip on a selected area. The tip material (commonly diamond or hard metal (WC)) is drawn across the borided surface under constant, incremental or progressive load. At a certain critical load, the boride layer will start to fail. The critical loads are very precisely detected by means of an acoustic sensor attached to the load arm but can also be confirmed and collated with observations from a built-in optical microscope. The critical load data is used to quantify the adhesive properties of different boride layer-substrate combinations.

4. EXPERIMENTAL RESULTS AND DISCUSSIONS

4.1. SEM Observations of Boride Layers

Figure 6 gives the cross-sectional views of the boride layers formed on AISI 9840 steel at different temperatures for 8 h. The (boride layer/substrate) interface has a saw-tooth morphology and the boride layer looks very dense, continuous and uniform.

This particular morphology is observed when boriding Armco iron, carbon steels and low-alloy

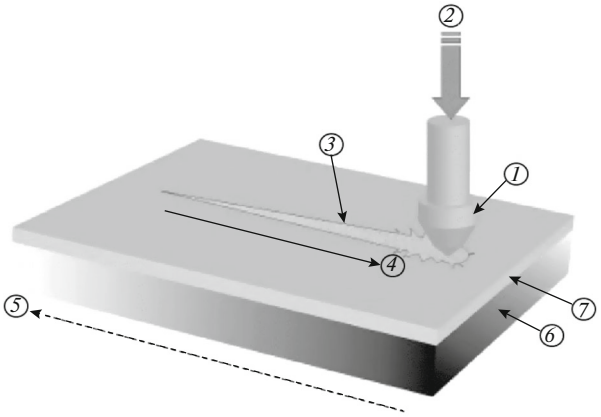

Fig. 5. Schematic diagram of typical scratch test device ((*1*) rockwell-C indenter; (*2*) weight (1 N, 2 N, 5 N, 10 N..., 90 N); (*3*) trail obtained; (*4*) tangent force; (*5*) horizontal displacement of the borided sample ($x(t)$); (*6*) substrate; (*7*) borided surface).

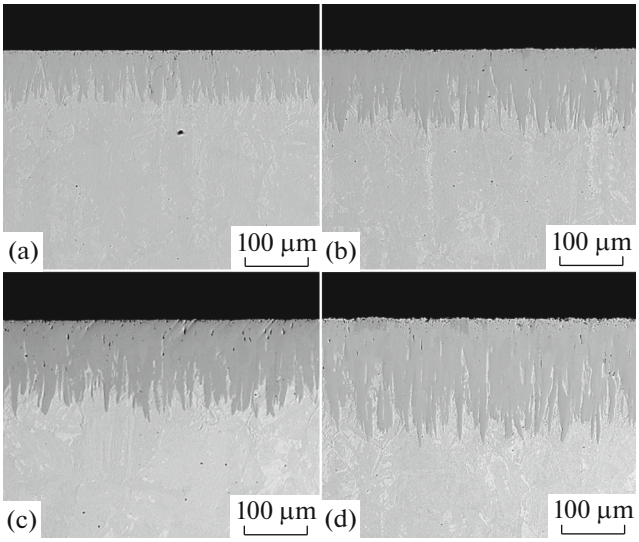

Fig. 6. SEM micrographs of the cross-sections of borided AISI 9840 steels for 8 h at different boriding temperatures: (a) 1123, (b) 1173, (c) 1223 and (d) 1273 K.

steels. It is reported that the growth of Fe_2B layer has a highly anisotropic nature and displays a [001] preferred crystallographic orientation [37] since the atom density of boron is maximum along this direction. Therefore, the boride grains with the [001] direction perpendicular to the surface of the sample grow faster aligned to the gradient of boron concentration. The boride layer thickness is increased as the boriding temperature rises.

This observed saw-tooth morphology is attributed to the presence of minor alloying elements in the AISI 9840 steel and can be explained by the existence of activated diffusion pathways in the Fe_2B crystal lattice [16]. The boride layer grows as needles in the AISI 9840 steel at the expense of stoichiometry of the compound layer Fe_2B and exhibited a highly anisotropic nature. The columnarity became more pronounced and a thicker boride layer was obtained with a rise of boriding temperature. In addition, the Fe_2B coating and its growth front are clearly distinguished from the steel matrix.

4.2. X-ray Diffraction Analysis

Figure 7 shows the XRD patterns obtained at the surfaces of borided AISI 9840 steels at a temperature of 1273 K for increasing treatment times (2, 6 and 8 h). The diffraction peaks relative to the Fe_2B phase are easily identified and have different intensities. It is recognized that the growth of Fe_2B is a controlled diffusion phenomenon with a highly anisotropic nature. The [001] direction is the easiest path for the boron diffusion in the body centered crystalline structure of the Fe_2B phase, due to the tendency of boride crystals to grow along a direction of minimum resistance, perpendicular to the external surface [37]. In addition no metallic borides were detected by XRD analysis at the surface of borided sample at 1273 K with 8 h of treatment. The formation of iron borides and metallic borides can be observed in the case of high – alloyed steels as reported by Genel [38] and Keddam et al. [16].

4.3. Rockwell-C Adhesion Test

Figure 8 shows the SEM micrographs after applying a conical diamond indenter (according to the VDI 3198 norm) on the surfaces of borided samples at 1123 K for two treatment times 2 and 8 h. The indentation craters obtained on the surfaces of the pack-borided AISI 9840 steel revealed that there were radial cracks at the perimeter of indentation craters. However, a

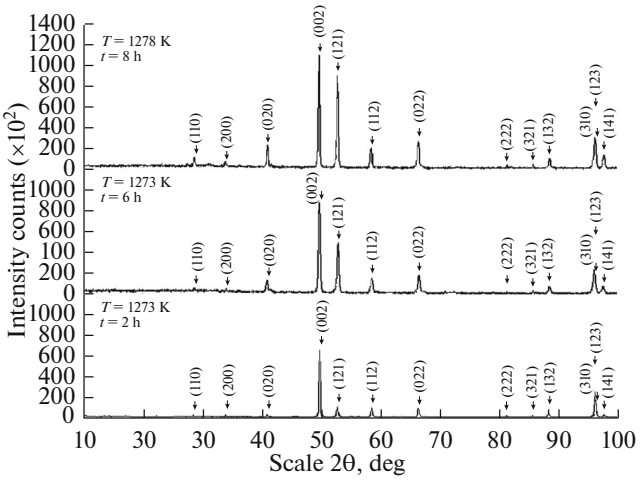

Fig. 7. XRD patterns obtained at the surfaces of the borided AISI 9840 steels at 1273 K for 2, 6 and 8 h of treatment.

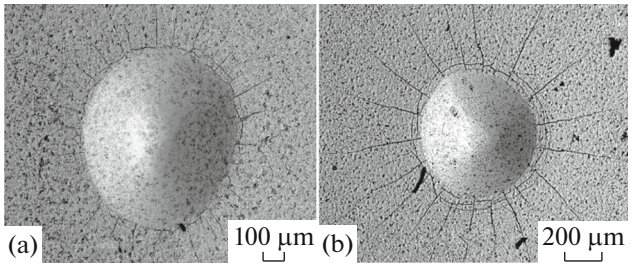

Fig. 8. SEM micrographs showing indentations of VDI adhesion test on surfaces of AISI 9840 steel borided at 1123 K for variable treatment times: (a) 2 and (b) 8 h.

small quantity of spots with flaking resulting from delamination was visible.

The adhesion strength quality of this boride layer is related to the HF3 standard. It is concluded that the presence of Fe_2B phase is responsible of improving the adhesion of boride coating on AISI 9840 steel. Furthermore, the boride layer on AISI 9840 steel treated at 1123 K for 2 h exhibited a better cohesion to the substrate when compared to the borided sample at 1123 K for 8 h. This fact can be explained by a reduced boride layer thickness obtained at 1123 K for 2 h. In this condition, the boride layer can endure the shear stresses at the (Fe_2B/substrate) interface and prevent the extended flaking failures circumferentially to the indentation carter. The author Taktak [36] showed that the interfacial cohesion of boride coatings depended on the boriding conditions on AISI H13 and AISI 304 steels. Kayali and Taktak [39] used the Daimler-Benz Rockwell-C adhesion test to identify the delamination failure characteristics of borided Cr-based steels. They showed that adhesion of boride layers depended on the dual-phase structure (FeB + Fe_2B). With increase in the depth of hard and brittle FeB-based layer, the stresses at the (FeB/Fe_2B) interface caused delamination failure and poor interfacial adhesion. The formation of a single boride layer Fe_2B promotes the cohesion quality of borided AISI 9840 steel. It was reported by Campos-Silva et al. [40] that the presence of a double boride layer (FeB + Fe_2B) on AISI H13 steel decreased the adherence of the coated system due to the presence of FeB with tensile residual stresses.

4.4. Microhardness Profiles

Figure 9a shows the cross-sectional indentation marks made along the boride layer formed at the surface of AISI 9840 steel at 1273 K for 8 h. Hardness-depth profiles obtained on the cross-sections of borided AISI 9840 steel for 6 h at different temperatures and under an applied load of 0.5 N are given in Fig. 9b.

At a distance close to 10 μm, from the surface of borided AISI 9840 steel, the hardness values of the

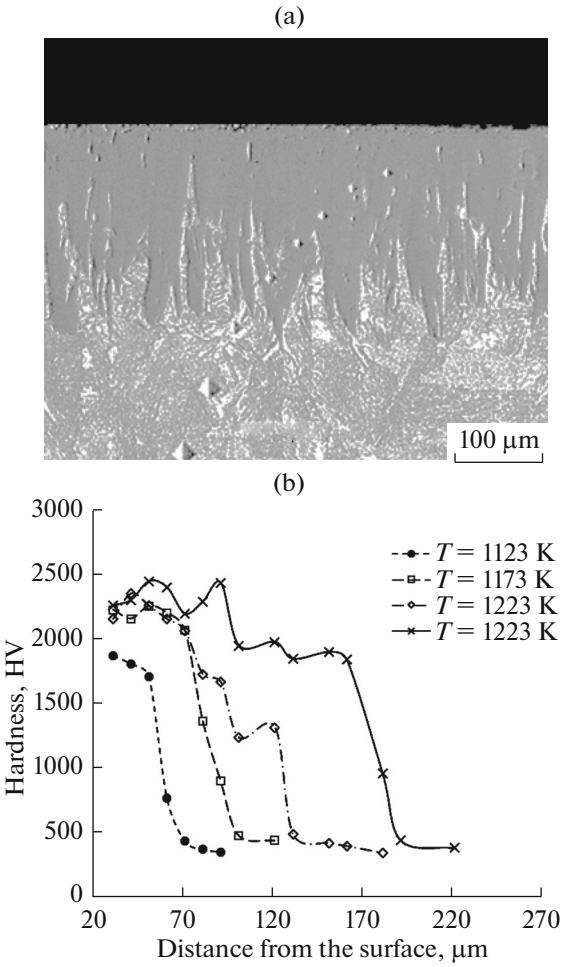

Fig. 9. (a) Vickers indentation marks along the cross-section of borided AISI 9840 steel at 1273 K for 8 h, (b) Hardness-depth profiles on the cross-sections of borided ASI 9840 steels at increasing temperatures during 6 h of treatment, under an applied load of 0.5 N.

borided samples approximately ranged from 1867 to 2445 HV under a load of 0.5 N. The estimated values of surface hardness of borided AISI 9840 steels are approximatively between 1867 and 2445 HV under an applied load of 0.5 N (at a distance close to 10 μm from the surface). The hardness-depth profiles can be correlated with the change in the boron concentration gradient. Hence, the diffusion front increased with the rise of boriding temperature as confirmed by SEM observations (see Fig. 6). It is obvious that the hardness-depth profiles are influenced by the boriding temperature for a given treatment time. It is also known that thermal residual stresses, arising from the growth of Fe_2B layer and the difference in specific volume can exert a significant effect on the hardness – depth profile. The hardness values at the surfaces of borided samples are found to be much high compared

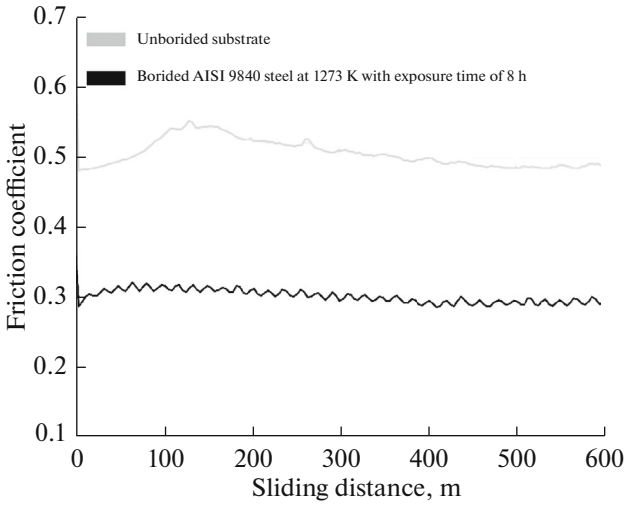

Fig. 10. Variation of the friction coefficient versus the sliding distance with a diamond indenter against the borided surface of AISI 9840 steel (at 1273 K for 8 h) and the unborided surface.

with the hardness of unborided sample due to the presence of Fe_2B phase.

In the case of Fe_2B layer, the hardness value was from 1867 to 2445 HV for the boriding temperatures of 1123, 1173, 1223 and 1273 K with an exposure time of 6 h (particularly, for these boriding conditions, the indentations were performed nearest the boride layer surface and the (boride layer/substrate) interface), the values of hardness tend to increase for 1123, 1173, 1223 and 1273 K. The apparent hardness is proportional to the residual compressive stress. The hardness is entirely caused by the increase in the residual compressive stress. In that case, in the first stage of boriding, a thin, compact boride layer forms on the surface followed by diffusion in the direction of the bulk, leading to an increased volume in the dimensional growth by 5 to 25% of the layer thickness and the residual compressive stress [41].

Different studies [42–46] have established that the hardness values of the iron borides are mainly affected by the following parameters: (the thermal residual stresses, the temperature and treatment time, the chemical composition of the substrate and the degree of anisotropy of the boride layer). In this context, Genel et al. [45] have investigated the pack – boriding of AISI W1 steel in the temperature range of 1123–1223 K. They found that the values of surface microhardness measured, at a depth of 10 μm below the surfaces of the cross-sections of borided samples, are increased with the boriding temperature up to approximatively 1223 K.

Ucar et al. [46] have obtained the microhardness profile measured on the cross-section of borided micro-alloyed steel at different temperatures for a treatment time of 4 h. They found that the microhardness values of boride layers are increased with increasing boriding temperatures due to the activation of diffusion of boron atoms.

4.5. The pin-on-disc test

Figure 10 shows the variation in the friction coefficient versus the sliding distance with a diamond indenter against the borided surface of AISI 9840 steel (at 1273 K for 8 h) and the unborided surface, under dry sliding conditions. It is seen that the borided sample exhibited a friction coefficient lower than that of the unborided substrate.

The evolution of friction coefficient of the borided surface (at 1273 K for 8 h) as a function of sliding distance, under dry conditions, was found to be in the range of 0.297–0.351. The coefficient friction for the untreated sample was between 0.497 and 0.534. These results agree with those obtained in other works [14, 15, 47–50]. The friction coefficient values obtained in this work for AISI 9840 steel are very comparable to the literature data. For example, Selçuk at al. [48] have obtained the values of variable friction coefficient ranging from 0.36 to 0.62 on carbon steels while Yanqiu Xia et al. [49] have found values around 0.5 under applied loads between 20 N and 100 N. Venkataraman and Sundararajan [50] have investigated the wear resistance of borided medium carbon steel and they have found a value of friction coefficient between 0.3 and 0.5 depending upon the slip speed. The authors Garcia-Bustos et al. [51] have used the four ball-test to evaluate the wear resistance and they have found a value of friction coefficient equal to 0.32 for borided steel (at 1223 K for 1 h) and 0.62 for the unborided steel under dry conditions and applied load of 147 N. Furthermore, the results reported by Garcia-Bustos et al. [51] showed that the borided AISI 52100 steel exhibited high wear resistance, and lubricating features in comparison with the untreated steel. It is concluded that the presence of Fe_2B layer improves the tribological behaviour of AISI 9840 steel because of the high hardness of Fe_2B phase. In addition, it is well known that the hardness of boride layer plays an important role in improving the wear resistance.

4.6. The Scratch Wear Test

Figures 11 gives the SEM images of unborided and borided surfaces (obtained at 1123 K for 8 h) after the scratch wear tests. Figure 11a–11c show for the unborided surfaces, the wear debris and scratching lines along the wear track. Some regions undergo the plastic deformation as a common wear mechanism. Figure 11d–11f show the wear scar formed on the borided surfaces where some scratching lines are observed.

Figures 12 gives the SEM micrographs of the worn surfaces of borided samples at 1123 and 1273 K for 6 h, respectively. Cracks that propagate in depth along the

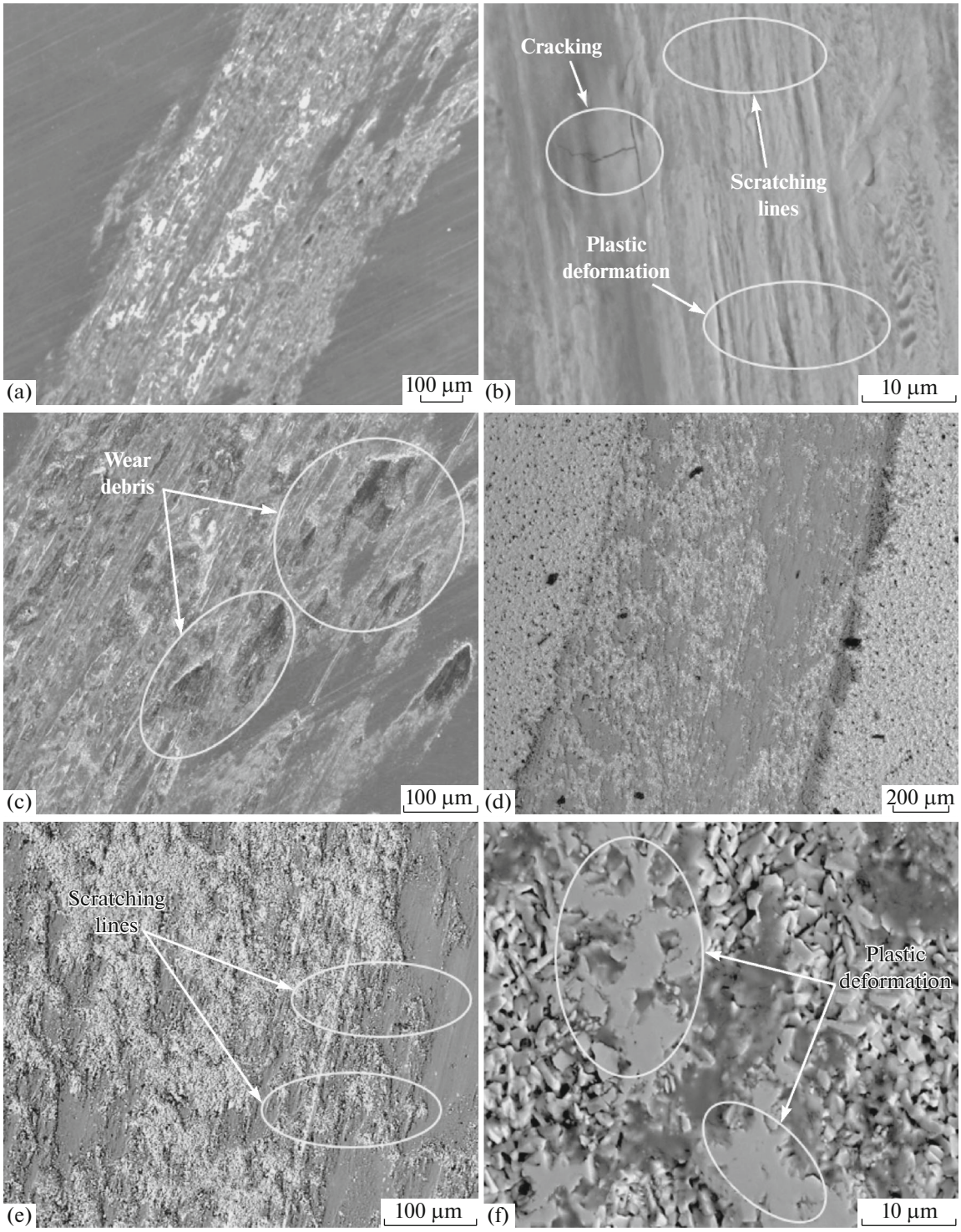

Fig. 11. SEM micrographs of wear scar on the surfaces of AISI 9840 steel: (a), (b) and (c) unborided surface and (d), (e) and (f) borided surface at 1123 K for 8 h.

scratch trails can be easily observed. They have either a curvilinear form (see Figure 12b) or a mosaic (see Figure 12d). According to the literature [52], this type of cracks is characteristic of a Hertzian fracture on brittle solids when a blunted indenter is used.

These cracks propagate in depth in a semi-conical shape and start at flaws near the contact surface where high-tension stresses develop [52, 53]. This was expected since it is well established that the coatings achieved at high temperature present a good interfacial

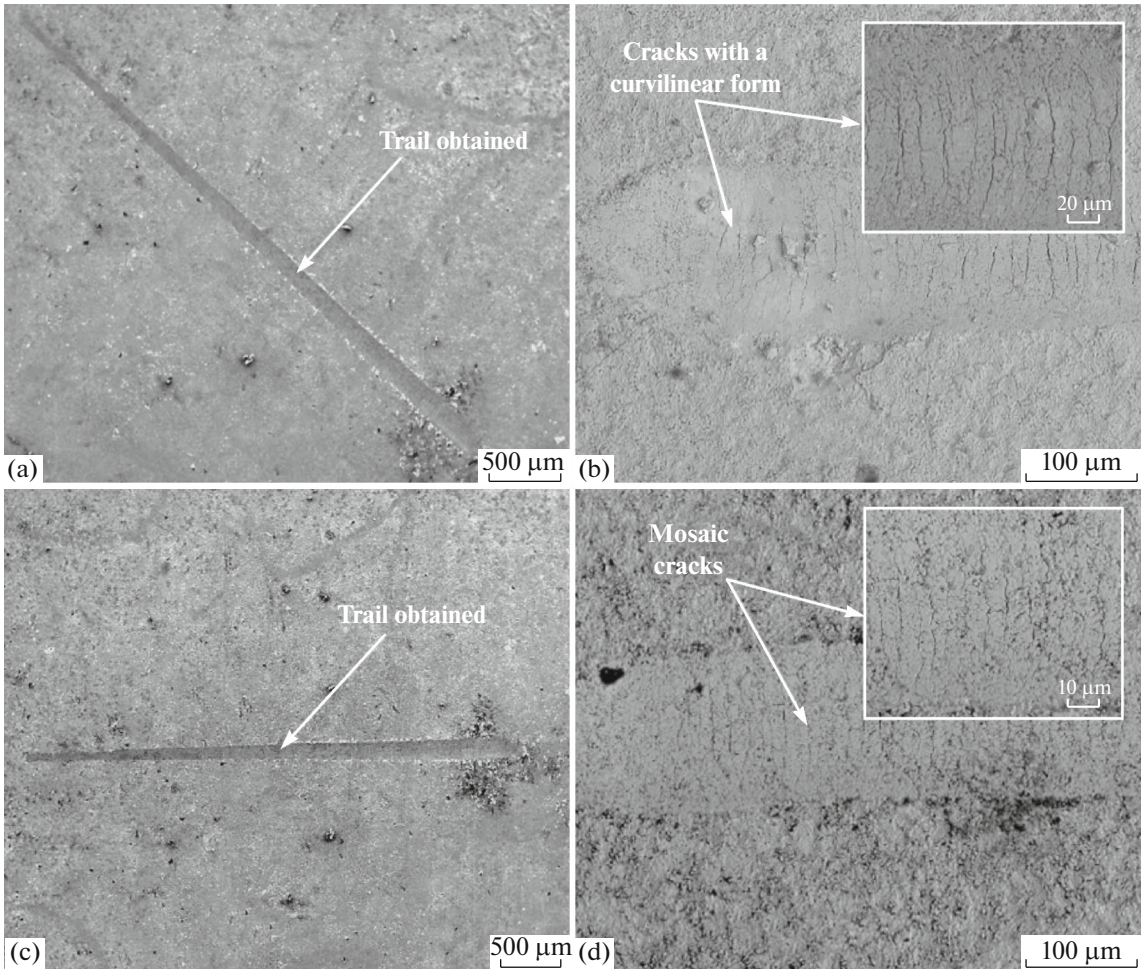

Fig. 12. SEM micrographs of wear scar on the surfaces of AISI 9840 steel for the following boriding conditions: (a) 1123 K for 6 h, (b) 1123 K for 6 h, (c) 1273 K for 6 h, and (d) 1273 K for 6 h.

adhesion because of the continuity of interface and chemical bonding between the boride coating and the substrate.

4.7. Estimation of Boron Activation Energy

To determine the boron activation energy for the AISI 9840 steel, it is necessary to solve the mass balance equation at the (Fe_2B/substrate) interface (see Eq. (11)). The determination of ε parameter is mandatory for obtaining the value of boron diffusion coefficient in the Fe_2B layers at each boriding temperature.

Figure 13 gives the evolution of the squared value of Fe_2B layer thickness versus the boriding time for different temperatures. The slopes of the straight lines plotted in Fig. 13 provide the values of growth constants ($=4\varepsilon^2 D_{Fe_2B}$). These values can be obtained by a linear fitting through origin at each boriding temperature. Table 1 displays the estimated value of boron diffusion coefficient in Fe_2B at each temperature along with the squared normalized value of ε determined from Eq. (11). The results, which are summarized in Table 1, reflect a diffusion-controlled growth of the boride layers.

By combining the results (square of normalized growth parameters (ε^2) and growth constants ($4\varepsilon^2 D_{Fe_2B}$)), the boron diffusion coefficient in the Fe_2B layers was estimated for each boriding temperature. So, the boron activation energy for the AISI 9840 steel was deduced from the slope of the straight line shown in Fig. 14.

A linear fitting was then adopted to obtain the temperature dependence of boron diffusion coefficient in Fe_2B with a correlation factor of 0.9934. The temperature dependence of boron diffusion coefficient through Fe_2B layers was given by Eq. (12):

$$D_{Fe_2B} = 2.07\times10^{-2}\exp\left(-\frac{193.08\ \text{kJ/mol}}{RT}\right), \quad (12)$$

where: $R = 8.314$ J/mol K and T the absolute temperature in Kelvin.

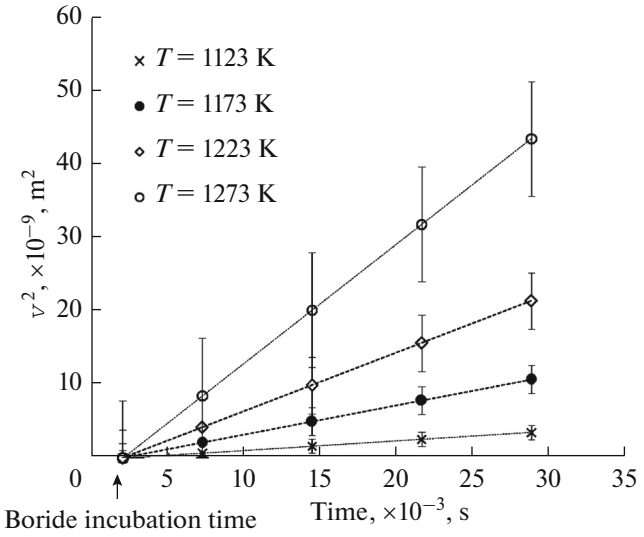

Fig. 13. The time dependence of the squared value of Fe_2B layer thickness for increasing temperatures.

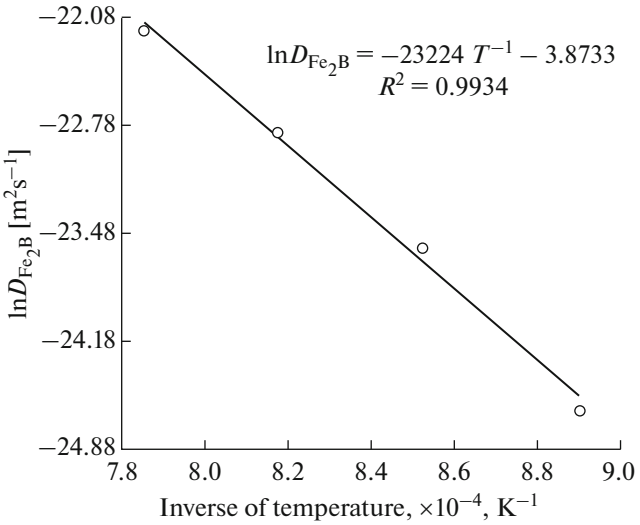

Fig. 14. The temperature dependence of boron diffusion coefficient in the Fe_2B layer.

As a result, a value of the boron activation energy for AISI 9840 steel was estimated as equal to 193.08 kJ mol^{-1}. Table 2 compares the value of boron activation energy for AISI 9840 steel with the values found in the literature for some borided steels and gray cast iron [18, 19, 38, 54–58].

The boron activation energy for the AISI 9840 steel was found to be equal to 193.08 kJ/mol. The value of energy can be interpreted, as the required amount of energy for the movement of boron atoms in the easiest path direction [001] along the boride layer that minimizes the growth stresses. Thus, the diffusion phenomenon of boron atoms can occur along the grains boundaries and also in volume to form the Fe_2B layer on the AISI 9840 steel. The estimated boron activation energies listed in Table 2 depended on various factors such as: (the nature of boriding agent, the boriding method, the mechanism of boron diffusion and the chemical composition of the substrate). So, an increase in the contents of alloying elements in the steel hinders the diffusion process of boron atoms by lowering the value of boron activation energy. Thus, the alloying elements present in the steel act as a diffusion barrier, reducing the diffusive flux of active boron atoms. Furthermore, the determination of the boron activation energies of the borided materials depends also on the method employed (either empirical approach or mathematical model).

However, some reported values of boron activation energies from the literature (see Table 2) for borided steels are very different. For indication, the value of boron activation energy obtained by Gunes et al. [57] on the AISI 8620 steel treated by the plasma paste boriding was in the range 124.7–138.5 kJ mol^{-1}. These values of boron activation energy are found to be lower when compared to the values listed in Table 2. It is observed that plasma paste boriding causes lower activation energy for the formation of boride layer than that of the conventional boriding process like the powder-boriding method.

4.8. Validation of the Diffusion Model

To extend the validity of the present model, additional boriding conditions were applied within the temperature range of 1123–1273 K. Figures 15 gives the SEM images of the cross-sections of Fe_2B layers formed on AISI 9840 steel at 1188 and 1248 K for 2 and 3 h, respectively.

Eq. (13) describes the evolution of boride layer thickness as a function of the boriding parameters (time and temperature) that was used to validate the present model used to validate the present model.

$$v = \sqrt{\frac{17 D_{Fe_2B} t}{2500}}. \quad (13)$$

Table 1. The squared value of normalized growth parameter and boron diffusion coefficients in Fe_2B versus the boriding temperature

Temperature, K	Type of layer	ε^2, Dimensionless	$4\varepsilon^2 D_{Fe_2B}$, $\mu m^2 s^{-1}$
1123	Fe_2B	1.747141×10^{-3}	1.405×10^{-1}
1173			4.05×10^{-1}
1223			8.56×10^{-1}
1273			16.27×10^{-1}

Table 2. A comparison of the boron activation energy of AISI 9840 steel with other steels and gray cast iron using different boriding methods

Material	Boriding method	Boron activation energy, kJ /mol	References
AISI 1045	Powder	180	[18]
Gray cast iron	Powder	184.2	[19]
AISI H13	Powder	186.2	[38]
SAE 1035	Salt-bath	227.51	[54]
Low carbon steel	Electrochemical	175.51	[55]
AISI 1018	Electrochemical	172.75 ± 8.6	[56]
AISI 8620	Plasma paste boriding	124.7–138.5	[57]
AISI 51100	Plasma	106	[58]
AISI 9840	Powder	193.08	Present study

Table 3. Predicted and estimated values of the Fe_2B layers thicknesses obtained at 1188 and 1248 K for the respective times of 2 and 3 h

Temperature, K	Type of layer	Boride layer thickness (μm) estimated by Eq. (16) for an exposure time of 2 h	Boride layer thickness (μm) estimated by Eq. (16) for an exposure time of 3 h	Experimental boride layer thickness (μm) for an exposure time of 2 h	Experimental boride layer thickness (μm) for an exposure time of 3 h
1188	Fe_2B	57.39	70.29	48.22 ± 6.4	75.93 ± 6.3
1248		91.82	112.24	98.37 ± 8.92	118.92 ± 10.4

The results obtained from Eq. (13) can be compared with the experimental values of Fe_2B layers thicknesses.

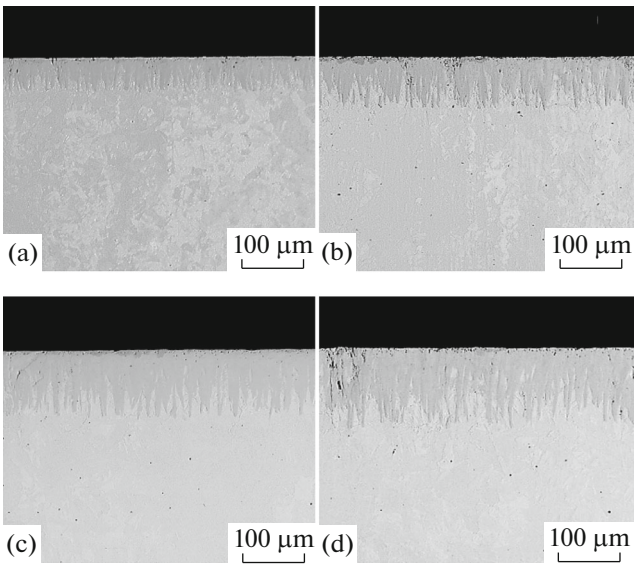

Fig. 15. SEM images of the cross-sections of borided AISI 9840 steels for different boriding conditions: (a) 1188 K for 2 h, (b) 1188 K for 3 h, (c) 1248 K for 2 h, and (d) 1248 K for 3 h.

Table 3 shows a comparison between the predicted values of Fe_2B layers thicknesses and the values experimentally obtained for the boriding conditions (1188 and 1248 K for 2 and 3 h, respectively). A good agreement was noticed between the experimental data and the predicted values for the given boriding conditions. Hence, Eq. (13) can be used to predict the optimum values of Fe_2B layer thickness as a function of boriding parameters (time and temperature) for practical applications of this kind of steel.

5. CONCLUSIONS

In this work, the AISI 9840 steel was subjected to the pack-boriding process in the temperature range of 1123–1273 K for a treatment time varying between 2 and 8 h. The Fe_2B layers were formed on AISI 9840 steel and its growth kinetics obeyed the parabolic growth law with the existence of boride incubation time independent on the boriding temperature.

A diffusion model was suggested to estimate the boron diffusion coefficient in Fe_2B in the temperature range of 1123–1273 K. As result, a value of activation energy for AISI 9840 steel was found to be equal to 193.08 kJ/mol. This result of boron activation energy was compared with the literature data.

To extend the validity of diffusion model, two additional boriding conditions were included. So, the obtained values of experimental Fe_2B layers thick-

nesses (at 1188 and 1248 K for 2 and 3 h, respectively) were compared with the predicted values. It is found that the experimental results agree with the predicted values by the model.

The interfacial adherence of the boride layer on AISI 9840 steel (obtained at 1123 K during 2 and 8 h), by the Daimler-Benz Rockwell-C indentation technique, was found to be related to HF3 category according to VDI 3198 norm. The microhardness values of Fe_2B near to the surface of borided samples for 6 h at different temperatures ranged from 1867 to 2445 HV.

For wear resistance, the average friction coefficient for the borided sample treated (at 1273 K during 8 h) was between 0.297 and 0.351 while the corresponding value of friction coefficient for the unborided sample ranged from 0.497 to 0.534. The decrease in friction coefficient of the treated sample was attributed to the formation of a hard layer of Fe_2B.

The wear mechanism of unborided sample was characterized by a plastic deformation along the wear track with an existence of debris and scratching lines. For the borided sample at 1123 K for 8 h, some pits and scratching lines were noticed.

ACKNOWLEDGMENTS

The work described in this paper was supported by a grant of CONACyT and PRODEP México. Also, the authors want to thank Ing. Martín Ortiz Granillo, who is in charge as *Director of the Escuela Superior de Ciudad Sahagún*which belongs to the Universidad Autónomadel Estado de Hidalgo, México, for all the facilities to accomplish this research work.

REFERENCES

1. Sinha, A.K., *J. Heat Treat.,* 1991, vol. 4, p. 437.
2. Bejar, M. and Moreno, E., *J. Mater. Process. Technol.,* 2006, vol. 173, p. 352.
3. Topuz, P., Gündoğdu, E., Yılmaz, E., and Gümüş, E., *Mater. Test.,* 2014, vol. 9, p. 690.
4. Jain, V. and Sundararajan, G., *Surf. Coat. Technol.,* 2002, vol. 149, p. 21.
5. Ulutan, M., Yildirim, M., Çelik, O., and Buytoz, S., *Tribol. Lett.,* 2010, vol. 38, p. 231.
6. Ozbek, I., *Arabian J. Sci. Eng.,* 2014, vol. 39, p. 5185.
7. Mathew, M. and Rajendrakumar, P., *Mater. Manuf. Processes,* 2014, vol. 29, p. 1073.
8. Kulka, M., Makuch, N., and Popławski, M., *Surf. Coat. Technol.,* 2014, vol. 244, p. 78.
9. Karakas, M.S., Ucar, N., and Unuvar, F., *Kovove Mater.,* 2014, vol. 52, p. 107.
10. Usta, M., Ozbek, I., Ipek, M., et al., *Surf. Coat. Technol.,* 2005, vol. 194, p. 330.
11. Kartal, G. and Timur, S., *Surf. Coat. Technol.,* 2013, vol. 215, p. 440.
12. Campos-Silva, I., Bravo-Bárcenas, D., et al., *Surf. Coat. Technol.,* 2013, vol. 237, p. 402.
13. Mu, D., Shen, B., and Zhao, X., *Mater. Des.,* 2010, vol. 331, p. 3933.
14. Elias-Espinosa, M., Ortiz-Domínguez, M., Keddam, M., et al., *Surf. Eng.,* 2015, vol. 31, p. 588.
15. Ortiz-Domínguez, M., Elias-Espinosa, M., Keddam, M., et al., *Indian J. Eng. Mater. Sci.,* 2015, vol. 22, p. 231.
16. Keddam, M., Ortiz-Domínguez, M., Elias-Espinosa, M., et al., *Trans. Indian Inst. Met.,* 2015, vol. 68, p. 433.
17. Flores-Rentería, M., Ortiz-Domínguez, M., Keddam, M., et al., *High Temp. Mater. Processes,* 2015, vol. 31, p. 1.
18. Zuno-Silva, J., Ortiz-Domínguez, M., Keddam, M., et al., *J. Min. Metall., Sect. B,* 2015, vol. 50, p. 101.
19. Ortiz-Domínguez, M., Flores-Rentería, M., Keddam, M., et al., *Mater. Tehnol.,* 2014, vol. 48, p. 905.
20. Elias-Espinosa, M., Ortiz-Domínguez, M., Keddam, M., et al., *J. Mater. Eng. Perform.,* 2014, vol. 23, p. 2943.
21. Ortiz-Domínguez, M., Keddam, M., Elias-Espinosa, M., et al., *Surf. Eng.,* 2014, vol. 30, p. 490.
22. Nait Abdellah, Z., Keddam, M., and Elias, A., *Int. J. Mater. Res.,* 2013, vol. 104, p. 260.
23. Nait Abdellah, Z., Keddam, M., Chegroune, R., et al., *Mater. Tech.,* 2012, vol. 100, p. 581.
24. Campos-Silva, I., Ortiz-Domínguez, M., Cimenoglu, H., et al., *Surf. Eng.,* 2011, vol. 27, p. 189.
25. Ortiz-Domínguez, M., Hernandez-Sanchez, E., Martínez-Trinidad, J., et al., *Kovove Mater.,* 2010, vol. 48, p. 1.
26. Keddam, M. and Chegroune, R., *Appl. Surf. Sci.,* 2010, vol. 256, p. 5025.
27. Keddam, M., Ortiz-Domínguez, M., Campos-Silva, I., and Martínez-Trinidad, J., *Appl. Surf. Sci.,* 2010, vol. 256, p. 3128.
28. Brakman, C.M., Gommers, A.W.J., and Mittemeijer, E.J., *J. Mater. Res.,* 1989, vol. 4, p. 1354.
29. Yu, L.G., Chen, X.J., Khor, K.A., and Sundararajan, G., *Acta Mater.,* 2005, vol. 53, p. 2361.
30. Okamoto, H., *J. Phase Equilib. Diffus.,* 2014, vol. 25, p. 297.
31. Nait Abdellah, Z., Chegroune, R., Keddam, M., et al., *Defect Diffus. Forum,* 2012, vol. 322, p. 1.
32. Dybkov, V.I., *Reaction Diffusion and Solid State Chemical Kinetics,* Zurich: *Trans. Tech. Publ.,* 2010, p. 7.
33. Kunst, H. and Schaaber, O., *HTM, Haerterei-Tech. Mitt.,* 1967, vol. 22, p. 275.
34. *Verein Deutscher Ingenieure Normen VDI 3198,* Dusseldorf: VDI-Verlag, 1991, p. 1.
35. Vidakis, N., Antoniadis, A., and Bilalis, N., *J. Mater. Process. Technol.,* 2003, vols. 143–144, p. 481.
36. Taktak, S., *Mater Des.,* 2007, vol. 28, p. 1836.
37. Palombarini, G. and Carbucicchio, M., *J. Mater. Sci. Lett.,* 1987, vol. 6, p. 415.
38. Genel, K., *Vacuum,* 2006, vol. 80, p. 451.
39. Kayali, Y. and Taktak, S., *J. Adhes. Sci. Technol.,* 2015, vol. 29, p. 2065.
40. Campos-Silva, I., Ortíz-Domínguez, M., et al., *Defect Diffus. Forum,* 2010, vol. 297, p. 1284.
41. Lin, Z., Wang, Z., and Sun, X., *Wear,* 1990, vol. 138, p. 285.

42. Galibois, A., Boutenko, O., and Voyzelle, B., *Acta Metall.,* 1980, vol. 28, p. 1753.
43. Campos-Silva, I., Ortíz-Domínguez, M., Tapia-Quintero, C., et al., *J. Mater. Eng. Perform.,* 2012, vol. 21, p. 1714.
44. Campos-Silva, I., Lopez-Perrusquia, N., Ortíz-Domínguez, M., et al., *Kovove Mater.,* 2009, vol. 47, p. 75.
45. Genel, K., Ozbek, I., and Bindal, C., *Mater. Sci. Eng., A,* 2003, vol. 347, p. 311.
46. Ucar, N., Aytar, O.B., and Calik, A., *Mater. Technol.,* 2012, vol. 46, p. 621.
47. Petrova, R.S., Suwattananont, N., and Samardzic, V., *J. Mater. Eng. Perform.,* 2006, vol. 17, p. 340.
48. Selçuk, B., Ipek, R., and Karamis, M.B., *J. Mater. Process. Technol.,* 2003, vol. 141, p. 189.
49. Yan-Qiu Xia, Wei-Min Liu, Lai-Gui Yu, et al., *Mater. Sci. Eng., A,* 2003, vol. 354, p.17.
50. Venkataraman, B. and Sundararajan, G., *Surf. Coat. Technol.,* 1995, vol. 73, p. 177.
51. Garcia-Bustos, E., Figueroa-Guadarrama, M.A., Rodriguez-Castro, G.A., et al., *Surf. Coat. Technol.,* 2013, vol. 215, p. 241.
52. Lawn, B.R., *J. Am. Ceram. Soc.,* 1998, vol. 81, p. 1977.
53. Allaoui, O., Bouaouadja, N., and Saindernan, G., *Surf. Coat. Technol.,* 2006, vol. 201, p. 3475.
54. Kaouka, A., Allaoui, O., and Keddam, M., *Mater. Tech.,* 2013, vol. 101, p. 705.
55. Matiasovsky, K., Chrenkova-Paucirova, M., Fellner, P., and Makyta, M., *Surf. Coat. Technol.,* 1998, vol. 35, p. 133.
56. Kartal, G., Eryilmaz, O., Krumdick, G., et al., *Appl. Surf. Sci.,* 2011, vol. 257, p. 6928.
57. Gunes, I., Taktak, S., Bindal, C., et al., *Sadhana,* 2013, vol. 38, p. 513.
58. Ipek, M., Celebi Efe, G., Ozbek, I., et al., *J. Mater. Eng. Perform.,* 2012, vol. 21, p. 733.